Electrostatic and Covalent Contributions in the Coordination Bonds of Transition Metal Complexes

Zhenhai Xiong,[†,‡] Yang Liu,[†] and Huai Sun*[,†]

School of Chemistry and Chemical Technology, Shanghai Jiao Tong University, Shanghai 200240, China, and College of Food Science and Technology, Shanghai Fisheries University, Shanghai 200090, China

Received: October 22, 2007; In Final Form: December 18, 2007

To develop a molecular mechanics force field for modeling complexes of transition metals and organic ligands, the electrostatic and covalent contributions in the coordination bonds were investigated using quantum mechanical density functional theory and model complexes of glyoxal diimine and the 2+ cations of the first row transition metals. The VDD and Hirshfeld charges are found to be closely correlated with the extent of the electron transfer between the ligands and the cations. Assuming the electrostatic contribution can be represented by the atomic partial charges, the covalent contributions in the coordination bonds are estimated to be in a range of 54−92% for the systems calculated. A simple force field was parametrized to validate the partial charge representation.

1. Introduction

The force field development for transition metal complexes has lagged significantly behind that for organic molecules or metal oxides. The challenges arise from the complexity of the electron structures that are often open shells and are influenced by multiple factors such as spin multiplicities, relativistic effects, and electron correlations. Large variations in the coordination bond lengths and angles exist for the same atom types. It is difficult to accurately represent the diversified interaction profiles using simple functional forms. Due to its great importance in potential applications, force fields for transition metal complexes have been proposed by several research groups.[1−5] However, the success of these force fields has been limited by their accuracy and applicability.

Most of the force fields for transition metal complexes reported in the literature are based on one of two models.[1] In one of the approaches the coordination bonds are treated as covalent bonds—the connectivity of each atom is known and fixed prior to and during the calculations. By adjusting the force field parameters, one can predict the structures of the complexes with reasonable success. However, this model lacks information about the energetic changes of bond dissociation and formation. An alternative approach is to treat the interactions between the transition metal and ligands as nonbond interactions which consist of the electrostatic (Columbic) and van der Waals (VDW) energy terms. In this approach, the transition metal atoms are usually treated as ions bearing formal charges, and the VDW energy terms are used as balance forces to fit the structural and energetic data of the complexes. In this model, the coordination bonds are dissociable. However, the models are too simple to represent the diversified structures of transition metal complexes accurately.

Ample data show that the metal−ligand bonds are not purely ionic even for highly polarized bonds.[6,7] From molecular orbital analyses it is clear that the coordination bonds are formed by orbital overlaps and electron donations between the ligands and transition metals. Therefore, it is reasonable to assume the coordination bonds can be represented by a combination of covalent and ionic contributions.[8] The challenge is, consequently, how to divide the contributions to the two categories. As the first step toward developing an accurate force field for transition metals complexes, we seek a way to represent the coordination bonds using both covalent and electrostatic components in this work.

For this purpose, a group of transition metal complexes consisting of the first-row transition metal 2+ cations and glyoxal diimine ligands, $[M(glyoxaldiimine)_3]^{2+}$, were analyzed for their electronic structures and potential energy surfaces. In addition to their simplicity, these model compounds represent six-coordinated octahedral complexes which are important moieties in polypyridine ligands found in many applications such as artificial photosynthesis,[9] donor sensitizer−acceptor arrays,[10−14] membrane-bound,[15−16] intrazeolitic,[17] polymeric,[18] DNA-intercalating,[19−22] or interacting with monoclonal antibodies.[23] A force field developed for these model compounds can be useful for these research fields.

2. Method

The compounds are in the D_3 symmetry as illustrated in Figure 1. There are six equivalent coordination bonds between the nitrogen atoms of the ligands and the transition metal cation at the center of the complex.

Density functional theory (DFT) calculations were performed using the ADF 2005 program package.[24−37] The Vosko−Wilk−Nusair (VWN)[35] exchange correlation functional with the nonlocal Becke exchange[34] and Perdew correlation corrections[36] were applied. The TZ2P basis set[24−40] with frozen core was applied in the calculations. The relativistic effects were investigated by using the zero-order regular approximation (ZORA) methods.[41−45]

The structures of the model compounds were optimized with symmetry constraints. The obtained structures were verified to

* To whom correspondence should be addressed. E-mail: huaisun@sjtu.edu.cn.
† Shanghai Jiao Tong University.
‡ Shanghai Fisheries University.

10.1021/jp710217p CCC: $40.75
Published on Web 02/28/2008

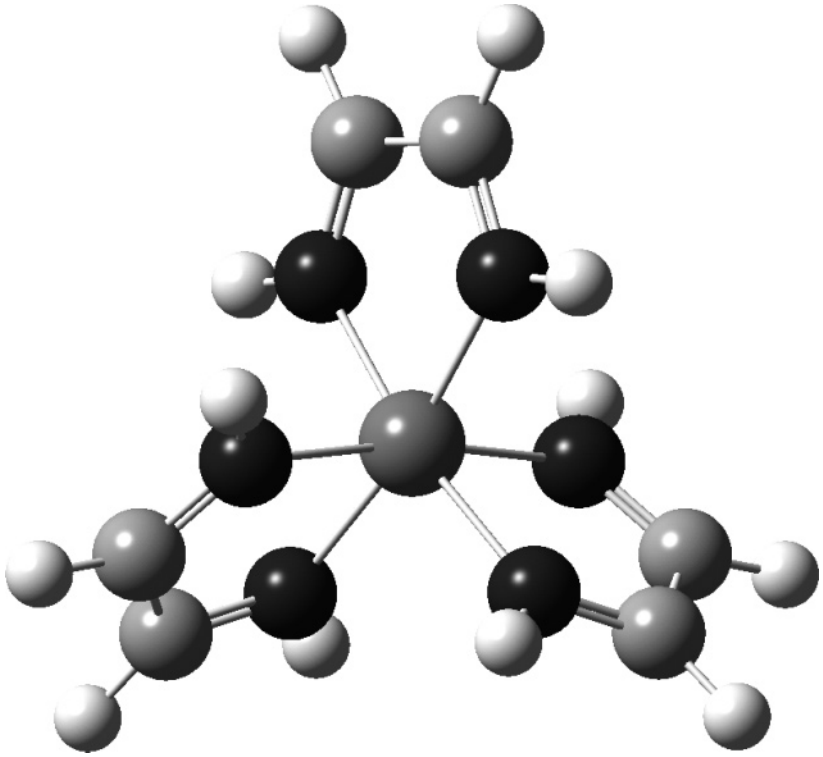

Figure 1. Structure of the $M^{2+}L_3$ (L = glyoxal diimine) complexes.

be minimum energy states using normal-mode analysis. On the basis of the optimized structures, the electron structures, charge transfers, and energy decompositions were analyzed. The fragment-based approach was taken in these calculations and analyses. For the geometry optimizations, each atom was treated as a fragment. For the subsequent energy and orbital analyses, each transition metal cation was defined as a fragment and the cluster of three ligand molecules was defined as another fragment.

The scheme developed by Ziegler and Rauk[46,47] was used for the energy decomposition analysis. In this approach, the total interaction energy between two fragments is decomposed into three terms:

$$\Delta E_{\text{int}} = \Delta E_{\text{elstat}} + \Delta E_{\text{Pauli}} + \Delta E_{\text{orb}}$$

The ΔE_{elstat} is the "rigid" electrostatic interaction energy between the fragments, which is calculated from the wave functions of the fragments in separation. ΔE_{Pauli} is the Pauli repulsive energy (electrons with the same spin cannot occupy the same region in space) between the fragments. The orbital interaction energy, ΔE_{orb}, is the interaction energy of the occupied orbitals on one fragment and unoccupied orbitals on another.

The Mayer bond order method[48] is popular for estimating the covalent contributions.[49−52] It was used in this work for comparison and analysis. To estimate the atomic charges, we carried out NBO,[53−55] Hirshfeld,[56] Voronoi deformation density (VDD),[57] and Mulliken[58] population analyses.

3. Results and Discussion

3.1. Energies and Structures. The relative energies of the 10 complexes in different spin multiplicities (from 1 to 7) are listed in Table 1. The lowest energy states obtained can be interpreted using the ligand field theory.[59−62] Under the D_3 symmetry, the third orbitals of the transition metal are split into two energy levels in the ligand field. Three orbitals are in lower energy, and two are in higher energy. The three low-energy orbitals are occupied first from Sc^{2+} to V^{2+}, yielding the multiplicity of 2−4, respectively. The next three d-electrons (from Cr^{2+} to Fe^{2+}) are in the low-energy level and the multiplicities are 3, 2, and 1. From Co^{2+}, the remaining 4 electrons are filled into the high-energy level, yielding multiplicities of 2, 3, 2, and 1, respectively. This pattern indicates the coordination field induced by the ligands is so strong that the splitting energy is higher than the pairing energy. However, it should be noted that alternative spin states are only a few kcal/mol higher than the ground state in many of the complexes.

TABLE 1: Number of d-Electrons (N_d), Relative Energies (in kcal/mol), and Spin Multiplicities (in Parentheses) of the First Three Energy Levels Calculated for the $M^{2+}L_3$ (L = Glyoxal Diimine) Complexes

M^{2+}	N_d	E_0	E_1	E_2
Sc^{2+}	1	0.0 (II)	72.2 (IV)	129.8 (VI)
Ti^{2+}	2	0.0 (III)	5.0 (I)	76.1 (V)
V^{2+}	3	0.0 (IV)	9.5 (II)	82.9 (VI)
Cr^{2+}	4	0.0 (III)	13.9 (V)	16.1 (I)
Mn^{2+}	5	0.0 (II)	31.9 (IV)	35.3 (VI)
Fe^{2+}	6	0.0 (I)	29.7 (III)	45.4 (V)
Co^{2+}	7	0.0 (II)	17.2 (IV)	67.8 (VI)
Ni^{2+}	8	0.0 (III)	21.8 (I)	57.9 (V)
Cu^{2+}	9	0.0 (II)	26.6 (IV)	100.4 (VI)
Zn^{2+}	10	0.0 (I)	63.8 (III)	115.8 (V)

The most characteristic bond lengths of the optimized complexes are given in Figure 2. As the number of the d-electrons (N_d) increases, the metal−nitrogen bond (M−N) lengths vary significantly between 1.9 and 2.3 Å. The curve shows an asymmetric V shape—it decreases monotonically from Sc^{2+} ($N_d = 1$) to Fe^{2+} ($N_d = 6$) and increases from Co^{2+} ($N_d = 7$) to Zn^{2+} ($N_d = 10$). On the other hand, the bond lengths of the ligand molecules N−C, C−H, and C−C are relatively stable.

The bond angles between the ligand nitrogen atoms and the cation (N−M−N) are illustrated in Figure 3. The angle in which both nitrogen atoms are in the same ligand molecule is denoted with α. Three angles are formed with the adjacent nitrogen atoms in different ligand molecules; one is denoted by β_1, and

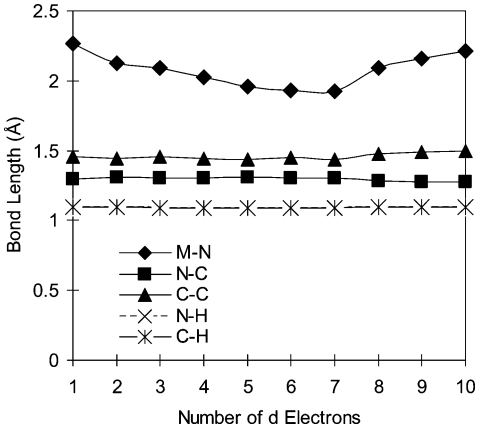

Figure 2. Optimized bond lengths as functions of the number of d-electrons in the complexes calculated. The metal cation and nitrogen bond lengths change significantly, and intramolecular bond lengths in the ligand molecules are relative stable.

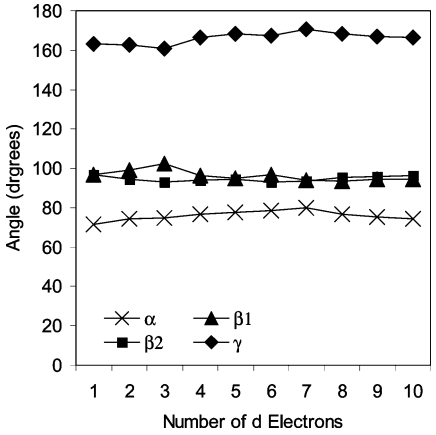

Figure 3. Optimized N−M−N angles as functions of the number of d-electrons in the complexes calculated. The α angle is defined for both nitrogen atoms are in the same ligand. The β angles formed as two nitrogen atoms are in different ligands but in adjacent positions. The γ angle is defined as two nitrogen atoms that are in different ligands and at the opposite positions.

other two, denoted by β_2, are identical due to symmetry. Finally, γ indicates the angle formed between opposite nitrogen atoms in different ligands. The angles α, β_1, β_2, and γ are about 80, 100, 100, and 160°, respectively, showing distorted octahedral structures. Unlike the bond lengths, these angles do not show a clear pattern of changes. The values are scattered within 10° from its average values.

The binding energies of the complexes are plotted in Figure 4. The energies are calculated as the energy differences between the optimized complexes and the corresponding fragments (cations M^{2+} and the ligands) optimized as isolated molecules. The binding energies are strong, in the range of −390 to −520 kcal/mol, which correspond to 65−87 kcal/mol for each of the coordination bonds. It is of interest to note that these values are comparable with the strengths of the double bonds in organic molecules. The relativistic corrections are also given in the figure. They are in the range of 2.5−8.7 kcal/mol, which are only about 1% of the total binding energies.

The binding energy curve does not correlate with the curve of the coordination bond lengths. Although the most stable complex $[Co(en)_3]^{2+}$ ($N_d = 7$) has the shortest N−M bond length, another molecule, $[Mn(en)_3]^{2+}$ ($N_d = 5$), is clearly off the pattern. This is because the binding energy is the energy difference between the complex and their corresponding fragments. The value is determined by two factors: the strength of

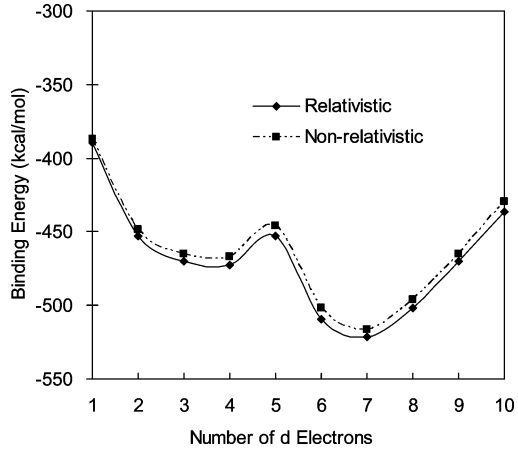

Figure 4. Binding energies of the cations and the ligands of the complexes as calculated by subtracting the total energy of the complexes by the corresponding total energies of the ligand clusters and cations. The relativistic corrections are included for comparison.

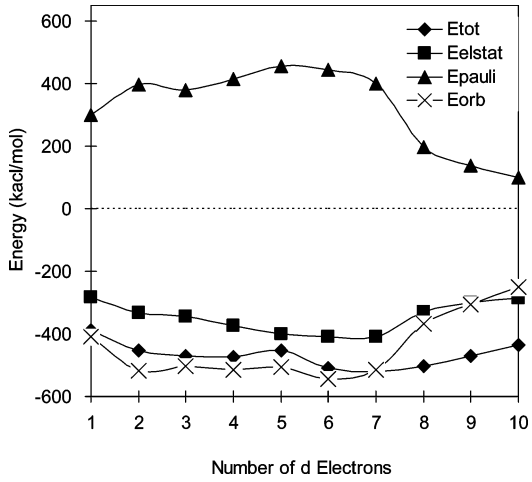

Figure 5. Energy decompositions for the complexes in terms of electrostatic, Pauli, and orbital contributions.

the coordination bonds; the stability of the corresponding fragments in their isolation states. For example, $[Mn(en)_3]^{2+}$ ($N_d = 5$) has relatively weak binding energy because the corresponding cation Mn^{2+} is particularly stable with the half-filled d-shell.

The total binding energies are decomposed on the basis of the method proposed by Ziegler and Rauk.[41−45] The results are plotted in Figure 5, as the number of d-electrons changes. The results are generally in line with those reported in the literature. The positive Pauli energy is offset by the negative electrostatic and orbital energies; the total binding energy is about a half of the summation of the later two components. It is of interest to note that the magnitudes of these quantities change significantly. Since the electrostatic energy is calculated from the undistorted electron densities of the fragments, it changes in the same pattern as the M−N bond lengths (in Figure 2).

The orbital energies, ΔE_{orb}, which measures the interactions of occupied orbitals on one fragment and vacant orbitals on another, are further partitioned into different irreducible representations A1, A2, and E1 in Figure 6. The energy components in A2 are nearly constant and small, indicating the A2 orbitals do not contribute significantly into the coordination bonds. An analysis of the electron density of the A2 orbitals of the ligand fragment and the cations reveals that the interaction is symmetrically unfavorable. On the other hand, both E1 and A1 orbitals are heavily involved in forming the coordination bonds.

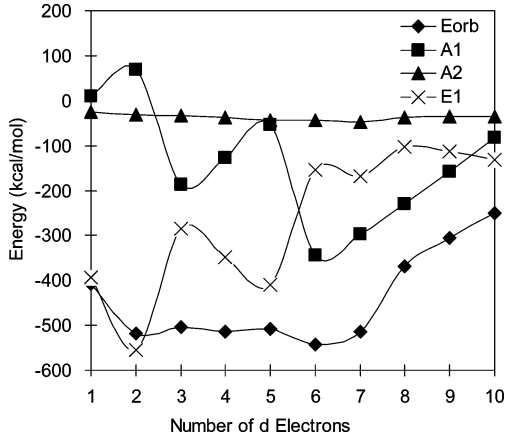

Figure 6. Orbital interaction energies decomposed into irreducible representations.

3.2. Orbital Analysis and Charge Distribution. An analysis of the molecular orbitals that contain at least 5% contributions from both metal and ligand fragments reveals the nature of the coordination bonds. The data are given in the Supporting Information; here we summarize the main results obtained from this analysis. The 3d, 4s, and 4p orbitals of the metal fragments are components of the molecular orbitals for the coordination bonds. The 3d orbitals are partially occupied except in the Zn^{2+} ($N_d = 10$) complex. The 4s and 4p ($4p_x$, $4p_y$, and $4p_z$) orbitals are unoccupied. These unoccupied or partially occupied orbitals interact with the occupied orbitals of the ligands, forming normal coordination bonds by donating electrons from the ligands to the metal cations. Two unoccupied orbitals of the ligands (12E1, π^*; A6, σ^*) are involved in the coordination bonds. These orbitals interact with the partially occupied or occupied 3d orbitals on the metal fragments to form π^* back-donation or σ^* back-donation bonds. From Sc^{2+} ($N_d = 1$) to Fe^{2+} ($N_d = 6$) the resulting π^* back-donation orbitals are bonding orbitals and occupied, but the percentage contribution of the ligand (12E1, π^*) orbital is decreasing for the series. From Co^{2+} ($N_d = 7$) to Zn^{2+} ($N_d = 10$), the resulting orbital is antibonding in nature. For Co^{2+} ($N_d = 7$), it is partially (one electron) occupied. For the last three cations in the period, this orbital is unoccupied. The σ^* back-donation orbitals are highly localized, indicating weak back-donation. As the number of d-electron increases, the $3d_{z^2}$ orbital gradually interacts with lower energy and occupied (A5 and A4) orbitals on the ligands and the σ^* back-donation disappears after Co^{2+}, similar to the case of the π^* back-donation.

Generally, the back-donations are associated with the number of d-electrons on the metal fragments. With few d-electrons, the energy levels of the 3d orbitals are close to the unoccupied ligand orbitals (12E1 and 6A1); as the number of d-electron increases, the energy levels of the 3d orbitals decrease and the energy gaps between the 3d orbitals and the occupied ligand orbitals decreases. As the number of d-electron is greater than 7 (Co^{+2}), the 3d orbitals mainly interact with the occupied ligand orbitals.

The above orbital analysis explains the changes in binding energies. In Figure 5, a sudden change in both Pauli repulsion and orbital interaction energies starting from Ni^{2+} ($N_d = 8$) is observed. This is correlated with the missing of the π^* or σ^* back-donation. The observed coordination bond lengths can also be understood using the electron configurations. From Sc^{2+} to Co^{2+}, the bond strength between the metal ion and ligands gradually increases, through orbital overlap, electron donation, and back-donation, and the bond lengths of M−N decreases monotonically. Starting from Ni^{2+}, the back-donations stops; the 3d orbitals interact with occupied ligand orbitals, resulting in antibonding orbitals. Consequently, the bond lengths of M−N increase.

The electron donation and back-donation were quantified by calculating the increments of occupation numbers in the unoccupied or partially occupied orbitals of the ligand and metal fragments. The results are listed in Table 2. On the metal cations, more electrons are gained as the number of d-electrons increases. Note that the greatest increments are on the 4s and 4p orbitals. The back-donations mainly transfer the electrons from the metal cations to the ligand π^* orbitals (12E1). From the Sc^{2+} ($N_d = 1$) to Co^{2+} ($N_d = 7$) complexes, the increments are relatively stable in the range 0.85−1.20 electrons. However, the back-donation disappears in the last three complexes. The differences between the two types of donations are given in the last column. A negative value indicates a net back-donation, which is only significant for the first two cations, Sc^{2+} ($N_d = 1$) to Ti^{2+} ($N_d = 2$).

The atomic charges are not physically observables, and consequently, there is no objective way to make quantitative assignments of the atomic charges. For the purpose of the force field development, however, a representation that best describes the physical significance of the systems is required. The calculated partial charges on the metal cations are plotted in Figure 7. The values are significantly different among the different methods. By definition, the Hirshfeld and VDD analyses are consistent with the orbital analysis given above. As the number of d-electron increases, more electrons are transferred from the ligands to the cations and the cations become less positively charged, ranging from slightly above 2.0 to 1.3 electrons. The NBO charges do not fit this pattern. Although the Mulliken charges display this pattern in general,

TABLE 2: Electron Population Increments on Fragment Orbitals That Are Unoccupied or Partially Occupied (3d) from Isolated Fragments to the $M^{2+}L_3$ (L = Glyoxal Diimine) Complexes[a]

	M					L				
M^{2+}	$4P_{x,y}$	$4P_z$	4s	3d	tot.	7A1	6A2	12E2	tot.	net (M−L)
Sc^{2+}	0.27	0.04	0.12	0.01	0.44	0.01	0.01	0.84	0.86	−0.42
Ti^{2+}	0.33	0.12	0.13	0.04	0.62	0.01	0.02	1.14	1.17	−0.55
V^{2+}	0.35	0.14	0.16	0.21	0.86	0.01	0.02	0.82	0.85	0.01
Cr^{2+}	0.42	0.19	0.15	0.20	0.97	0.01	0.02	1.00	1.03	−0.06
Mn^{2+}	0.46	0.23	0.16	0.27	1.12	0.01	0.03	1.04	1.08	0.04
Fe^{2+}	0.51	0.26	0.19	0.38	1.34	0.01	0.03	0.80	0.84	0.50
Co^{2+}	0.57	0.32	0.23	0.32	1.44	0.01	0.03	1.16	1.20	0.24
Ni^{2+}	0.53	0.25	0.36	0.27	1.41	0.01	0.01	0.20	0.22	1.19
Cu^{2+}	0.57	0.27	0.39	0.40	1.63	0.01	0.01	0.08	0.10	1.53
Zn^{2+}	**0.52**	**0.24**	**0.53**	**−0.03**	**1.26**	**0.01**	**0.01**	**0.00**	**0.02**	1.24

[a] The last column, (M−L), represents the net charge transfer from the ligands (L) to the cation (M^{2+}) due to electron donations.

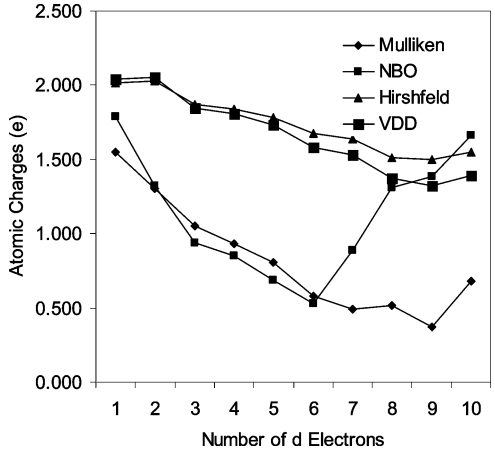

Figure 7. Atomic partial charges on the cations (M^{2+}) calculated using Mulliken, NBO, Hirshfeld, and VDD population methods.

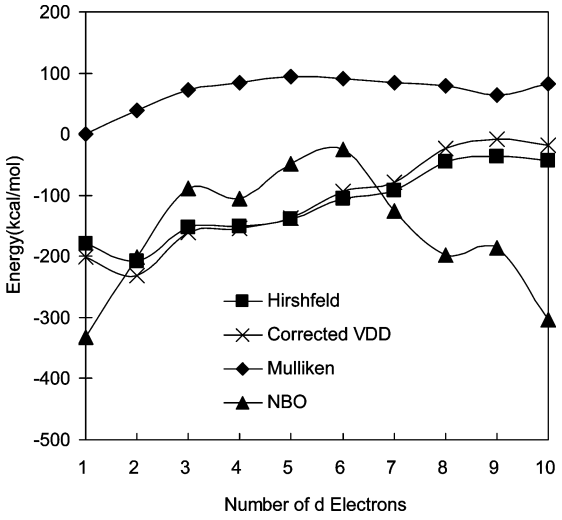

Figure 8. Electrostatic binding energies calculated using the partial charges obtained by different methods.

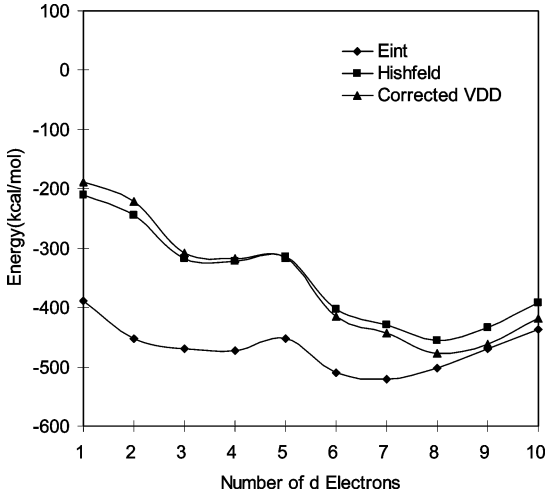

Figure 9. Valence binding energies as calculated by subtracting the electrostatic contributions (Figure 8) from the total bonding energies (Figure 4). The molecular structures are fixed to those optimized using the DFT calculations.

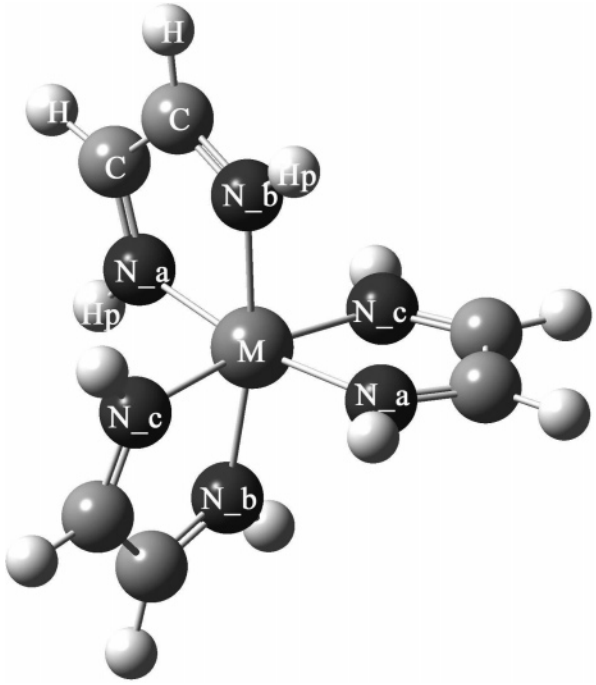

Figure 10. Atom types of molecules in our force field.

TABLE 3: Charge Parameters for Atoms in the $M^{2+}L_3$ (L = Glyoxal Diimine) Complexes Based on the Hishfeld Charges[a]

M^{2+}	M	N	C	HN	HC
Sc^{2+}	2.016	−0.312	0.068	0.140	0.102
Ti^{2+}	2.027	−0.315	0.063	0.141	0.106
V^{2+}	1.868	−0.297	0.070	0.143	0.107
Cr^{2+}	1.837	−0.290	0.064	0.145	0.108
Mn^{2+}	1.785	−0.281	0.061	0.146	0.110
Fe^{2+}	1.675	−0.268	0.066	0.147	0.110
Co^{2+}	1.638	−0.263	0.063	0.150	0.111
Ni^{2+}	1.514	−0.256	0.082	0.149	0.107
Cu^{2+}	1.499	−0.254	0.084	0.149	0.105
Zn^{2+}	1.547	−0.260	0.085	0.148	0.104

[a] M denotes the metal cations. N, C, HN, and HC are the nitrogen, carbon, and hydrogen bonded to the nitrogen and hydrogen bonded to the carbon, respectively.

TABLE 4: LJ-12−6 Parameters Used for the Atoms in the $M^{2+}L_3$ (L = Glyoxal Diimine) Complexes[a]

atom	ϵ	r_o
C	0.078	3.817
H(N)	0.010	1.000
H(C)	0.025	2.820
N	0.145	3.693
Sc^{2+}	0.019	3.295
Ti^{2+}	0.017	3.175
V^{2+}	0.016	3.144
Cr^{2+}	0.015	3.023
Mn^{2+}	0.013	2.961
Fe^{2+}	0.013	2.912
Co^{2+}	0.014	2.872
Ni^{2+}	0.004	2.834
Cu^{2+}	0.005	3.495
Zn^{2+}	0.124	2.763

[a] H(N) and H(C) denote hydrogen atoms bonded to nitrogen and carbon atoms, respectively.

the charges on the cations (ranging from 0.5 to 1.5 e) are significantly lower than the VDD and Hirshfeld values.

The electrostatic energies calculated using the partial charges provide another angle to evaluate the charge models. The calculated values, as displayed in Figure 8, show the Mulliken charges lead to positive electrostatic energies, indicating the electrostatic interactions make the complexes less stable. The energy curves calculated using the VDD and Hirshfeld charges

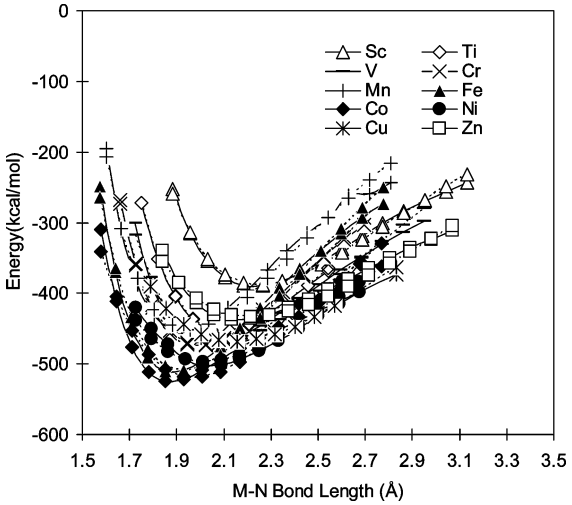

Figure 11. Comparison of symmetric stretch energy curves between the DFT results (dots) and the force field models (lines).

TABLE 5: Morse Parameters Optimized for Each Pair of the Interaction Terms between the Nitrogen and the Cation in the $M^{2+}L_3$ (L = Glyoxal Diimine) Complexes

pair	A	B	C
$N-Sc^{2+}$	34.649	1.341	2.483
$N-Ti^{2+}$	40.560	1.527	2.303
$N-V^{2+}$	53.439	1.246	2.287
$N-Cr^{2+}$	54.144	1.499	2.170
$N-Mn^{2+}$	52.269	1.618	2.104
$N-Fe^{2+}$	67.928	1.502	2.063
$N-Co^{2+}$	72.870	1.150	2.132
$N-Ni^{2+}$	75.790	0.964	2.187
$N-Cu^{2+}$	73.158	0.897	2.308
$N-Zn^{2+}$	65.939	0.891	2.395

are similar; both indicate a systematic raise of the electrostatic energies (decreasing in the strength) as the number of d-electrons increases.

To estimate the contribution of the covalent components in the coordination bonds, we subtracted the electrostatic energies from the total bonding energies and draw the results in Figure 9. We see that at beginning of the series (Sc^{2+}) the covalent contribution is about half of the total binding energy and gradually the covalent contribution increases. For the last three cations, the majority in the bonding energies are covalent in nature.

3.3. Force Field Model. To test if the partial charge model can be used in force field representations to describe the transition metal and organic ligand interactions, we made a potential function using the partial charge model. The interaction between the transition metal atom and nitrogen atoms of the ligands is represented with two parts: the Morse function for the covalence contribution and the Columbic term for the electrostatic contribution as follows

$$U_{\text{bond(metal-ligand)}} = A[(1 - \exp^{-B(r_{ij} - C)})^2 - 1] + \frac{q_i q_j}{r_{ij}} \quad (1)$$

For all other pair interactions we use LJ-12−6 and electrostatic terms:

$$U_{\text{nonbond}} = D\left[\left(\frac{E}{r_{ij}}\right)^{12} - 2\left(\frac{E}{r_{ij}}\right)^{6}\right] + \frac{q_i q_j}{r_{ij}} \quad (2)$$

To use the force field with common simulation engines, we applied common functional forms for bond, angle, and dihedral angle terms of the AMBER force field:

$$U_{\text{bond(ligand)}} = K_b(b - b_0)^2 \quad (3)$$

$$U_{\text{angle}} = K_\theta(\theta - \theta_0)^2 \quad (4)$$

$$U_{\text{dihedral}} = \frac{K_\phi}{2}[1 + \cos(n\phi - \phi_0)] \quad (5)$$

This imposes a challenge for representing the angles in which the transition metal atom is the vertex (N−M−N). Since this angle can be in three different ranges (around 70−80, 90−100, or 160−170°; see Figure 3), the angle function should have multiminima. Limited by the functional forms to be used, we utilized the definition of atom types to distinguish the variation of the angles. Figure 10 illustrates the definition of the atom types. With different combination of the atom types, the N−M−N angles can be represented with the simple harmonic function.

The VDD and Hirshfeld charge models reflect the extent of the electron transfer between the metal ions and the ligands. Both models perform similarly, as illustrated in Figures 7−9; either one can be used to represent the electrostatic interactions without changing the physical significance. In this work, we used the Hirshfeld charges in eqs 1 and 2. The ab initio charges were assigned to the transition metal atoms. The values of the carbon and hydrogen atoms in the ligands are calculated by averaging over all complexes. With these values fixed, the atomic charges of the nitrogen atoms in the ligands are calculated so that the total charge (2+) of the complex is conserved. The atomic charge parameters are listed in Table 3. The LJ parameters, as listed in Table 4, are taken from the OPLS force field[63−65] for the ligands and from UFF[66,67] for the cations.

With the charge and LJ parameters fixed, the Morse and other valence parameters were derived by fitting the DFT energy data. The energy surfaces were sampled by stretching the metal−

TABLE 6: Comparison of the N−M−N Angles (in deg) Calculated Using the DFT (QM) and the Force Field (MM)

angle	method	Sc^{2+}	Ti^{2+}	V^{2+}	Cr^{2+}	Mn^{2+}	Fe^{2+}	Co^{2+}	Ni^{2+}	Cu^{2+}	Zn^{2+}
α	QM	71.5	74.2	75	76.7	77.7	78.7	81	76.7	75.5	74.4
	MM	70.4	74.5	75.6	77.9	78.7	80.0	83.4	79.3	74.1	77.2
	diff	1.1	−0.3	−0.6	−1.2	−1.0	−1.3	−2.4	−2.6	1.4	−2.8
β_1	QM	115.6	107.7	104.9	98.2	95.1	97.3	93.5	94.8	95.4	96.8
	MM	109.8	101.2	99.7	94.7	94.3	94.8	92.5	94.4	94.6	95.1
	diff	5.8	6.5	5.2	3.5	0.8	2.5	1.0	0.4	0.8	1.7
β_2	QM	91.2	91.6	92	93.5	94.2	92.7	93	94.9	95.3	95.3
	MM	93.3	93.6	93.5	93.6	93.9	93.0	92.2	93.6	96.4	94.5
	diff	−2.1	−2.0	−1.5	−0.1	0.3	−0.3	0.8	1.3	−1.1	0.8
γ	QM	147.7	156.0	158.8	165.1	168.1	167.1	171.4	167.7	166.5	164.8
	MM	151.9	161.5	163.3	169.4	169.3	169.8	173.7	169.6	166.2	167.7
	Diff	−4.2	−5.5	−4.5	−4.3	−1.2	−2.7	−2.3	−1.9	0.3	−2.9

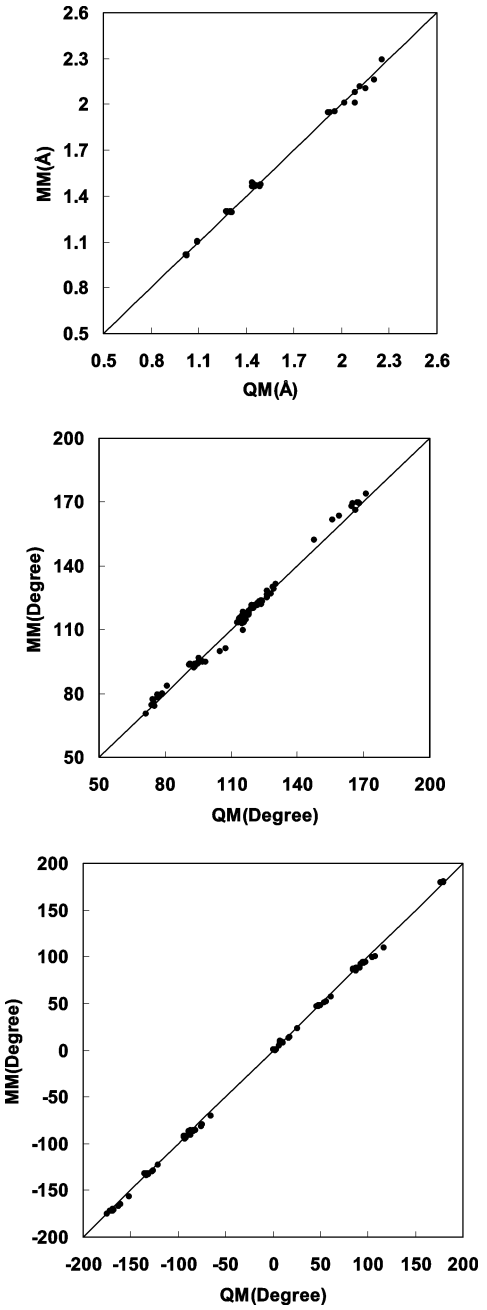

Figure 12. Comparison of bond lengths (a, in Å), bond angles (b, in deg), and dihedral angles (c, in deg) of the complexes predicted using DFT and the force field. The standard deviations are 0.02 Å for the bond lengths, 1.8° for bond angles, and 2.1° for dihedral angles. The maximum deviations are 0.07, 6.5, and 7.5, respectively.

ligand distances. The range of sampling was from −0.5 to 1.0 Å from the minimum energy distance with an interval of 0.1 Å. A total of 145 converged data points were obtained and used to fit the parameters. The optimized Morse parameters are given in Table 5, and other parameters are given in the Supporting Information. The well-depth parameters (Å) given in Table 5 are closely correlated to the strength of the covalence contribution (see Figure 9). As the number of the d-electrons increases, the covalence contribution increases. The covalent contribution in Sc^{2+} ($N_d = 1$) is about half of that in Zn^{2+} ($N_d = 10$).

A comparison of the bond-stretch energy curves between the ab initio and force field data is given in Figure 11. For the 145 data points ranging from −195.184 to −524.381 kcal/mol, the rms deviation is 9.8 kcal/mol. Close examination of the data shows that the errors are correlated with the energy values. Large errors are found in the high-energy ranges where the bonds are stretched or compressed. At the minimum energy vicinity, the agreement is much better. Table 6 lists comparisons of the coordination bond angles (N−M−N) between the ab initio and force field predictions. The force field results agree well with the ab initio data. More comparisons of the geometric data are given in Figure 12. Over all, the standard deviations are 0.02 Å for the bond lengths, 1.8° for the bond angles, and 2.1° for the dihedral angles. The maximum deviations are 0.07 Å, 6.5°, and 7.5°, respectively.

4. Conclusion

Using quantum mechanical DFT methods, we studied the total energies, binding energies, and molecular structures of model octahedral coordination complexes of glyoxal diimine ligands and 2+ cations of the first row transition metal elements. The spin states of the most stable electronic structures agree with the analysis of crystal field theory. The relativistic effects calculated are about 1% of the total binding energies. The structures of the complexes are generally distorted octahedral. As the number of d-electron increases in the series, the coordination bond lengths change significantly. The bond angles are relatively stable across the cations.

An analysis of the electron structures of the complexes indicates that the strength of electron donation from the ligands to the cations increases as the number of d-electrons of the cations increases. The back-donation (both π^* and σ types) from the cations to the ligands are near-constant up to seven d-electrons (Co^{2+}). For the last three cations (Ni^{2+}, Cu^{2+}, and Zn^{2+}) the back-donation is minimal. The combined effect is that increased electron transfer from the ligands to cations as the number of d-electrons increase.

The atomic partial charges calculated using the VDD and Hirshfeld methods are consistent with the electron-transfer scheme obtained from the orbital analysis. However, the atomic partial charges obtained using the Mulliken and NBO methods are not in the same pattern. With the VDD and Hirshfeld charges the electrostatic contributions in the coordination bonds range from −220 to −20 kcal/mol, which are about 46% to 8% of the total binding energies.

A simple force field that uses atomic partial charges for the electrostatic and Morse function for the covalence contributions was parametrized to test if the partial charge model can be used for modeling transition metal ligand complexes. For coupling with classical force field functions, we found this force field fits the QM data well. This is however the first step toward developing an accurate force field for organic ligand and transition metal complexes. Many issues need to be considered. Among them, how to represent the complex structures is one of critical problems to be solved. In this work, we used the definitions of different atom types to compromise the inadequacy of functional forms. This is largely limited by the avalibility of simulation software. Further investigation seeking the best functional form is being undertaken.

Acknowledgment. Financial support from the National Science Foundation of China (Grants 20473052, 10676021) and National Basic Research Program of China (Grants 2003CB615804, 2007CB209700) is gratefully acknowledged.

Supporting Information Available: Molecular orbitals that contain major contributions from the fragment orbitals and the force field parameters derived on the basis of the ab initio

calculations. This information is available free of charge via the Internet at http://pubs.acs.org.

References and Notes

(1) Brandt, P.; Norrby, T.; Akermark, B.; Norrby, P.-O. *Inorg. Chem.* **1998**, *37*, 4120−4127.
(2) Oda, A.; Yamaotsu, N.; Hirono, S. *J. Comput. Chem.* **2005**, *26*, 818−826.
(3) Hagelin, H.; Svensson, M.; Akermark, B.; Norrby, P.-O. *Organometallics* **1999**, *18*, 4574−4583.
(4) Ledecq, M.; Lebon, F.; Durant, F.; Giessner-Prettre, C.; Marquez, A.; Gresh, N. *J. Phys. Chem. B* **2003**, *107*, 10640−10652.
(5) Gresh, N.; Policar, C.; Giessner-Prettre, C. *J. Phys. Chem. A* **2002**, *106*, 5660−5670.
(6) Bickelhaupt, F. M.; van Eikema Hommes, N. J. R.; Guerra, C. F.; Baerends, E. J. *Organometallics* **1996**, *15*, 2923−2931.
(7) Diefenbach, A.; Matthias Bickelhaupt, F.; Frenking, G. *J. Am. Chem. Soc.* **2000**, *122*, 6449−6458.
(8) Zhao, L.; Liu, L.; Sun, H. *J. Phys. Chem. C* **2007**, *111*, 10610−10617.
(9) Meyer, T. J. *Acc. Chem. Res.* **1989**, *22*, 163−170.
(10) Opperman, K. A.; Mecklenburg, S. L.; Meyer, T. J. *Inorg. Chem.* **1994**, *33*, 5295−5301.
(11) Harriman, A.; Odobel, F.; Sauvage, J.-P. *J. Am. Chem. Soc.* **1995**, *117*, 9461−9472.
(12) Coe, B. J.; Thompson, D. W.; Culbertson, C. T.; Schoonover, J. R.; Meyer, T. J. *Inorg. Chem.* **1995**, *34*, 3385−3395.
(13) Barigelletti, F.; Flamigni, L.; Balzani, V.; Collin, J.-P.; Sauvage, J.-P.; Sour, A.; Constable, E. C.; Cargill Thompson, A. M. W. *J. Am. Chem. Soc.* **1994**, *116*, 7692−7699.
(14) Constable, E. C.; Cargill Thompson, A. M. W.; Tocher, D. A.; Daniels, M. A. M. *New J. Chem.* **1992**, *16*, 855−867.
(15) Clapp, P. J.; Armitage, B.; Roosa, P.; O'Brien, D. F. *J. Am. Chem. Soc.* **1994**, *116*, 9166−9173.
(16) Sabatini, E.; Nikol, H. D.; Gray, H. B.; Anson, F. C. *J. Am. Chem. Soc.* **1996**, *118*, 1158−1163.
(17) Ledney, M.; Dutta, P. K. *J. Am. Chem. Soc.* **1995**, *117*, 7687−7695.
(18) Bergstedt, T. S.; Hauser, B. T.; Schantze, K. S. *J. Am. Chem. Soc.* **1994**, *116*, 8380−8381.
(19) Arkin, M. R.; Stemp, E. D. A.; Turro, C.; Turro, N. J.; Barton, J. K. *J. Am. Chem. Soc.* **1996**, *118*, 2267−2274.
(20) Meade, T. J.; Kayyem, J. F. *Angew. Chem., Int. Ed. Engl.* **1995**, *34*, 352−354.
(21) Lincoln, P.; Broo, A.; Nordeń, B. *J. Am. Chem. Soc.* **1996**, *118*, 2644−2653.
(22) Campisi, D.; Morii, T.; Barton, J. K. *Biochemistry* **1994**, *33*, 4130−4139.
(23) Shreder, K.; Harriman, A.; Iverson, B. L. *J. Am. Chem. Soc.* **1996**, *118*, 3192−3201.
(24) te Velde, G.; Bickelhaupt, F. M.; Gisbergen, S. J. A. v.; Guerra, C. F.; Baerends, E. J.; Snijders, J. G.; Ziegler, T. *J. Comput. Chem.* **2001**, *22*, 931−967.
(25) Guerra, C. F.; Visser, O.; Snijders, J. G.; te Velde, G.; Baerends, E. J. In *Methods and Techniques for Computational Chemistry*; Clementi, E., Corongiu, G., Eds.; STEF: Cagliari, Italy, 1995; p 305.
(26) Baerends, E. J.; Ellis, D. E.; Ros, P. *Chem. Phys.* **1973**, *2*, 41−51.
(27) Baerends, E. J.; Ros, P. *Chem. Phys.* **1975**, *8*, 412−418.
(28) Baerends, E. J.; Ros, P. *Int J. Quantum Chem. Symp.* **1978**, *12*, 169−190.
(29) Guerra, C. F.; Snijders, J. G.; te Velde, G.; Baerends, E. *J. Theor. Chem. Acc.* **1998**, *99*, 391−403.
(30) Boerrigter, P. M.; te Velde, G.; Baerends, E. J. *Int. J. Quantum Chem.* **1988**, *33*, 87−113.
(31) te Velde, G.; Baerends, E. J. *J. Comp. Phys.* **1992**, *99*, 84−98.
(32) Snijders, J. G.; Baerends, E. J.; Vernooijs, P. *At. Nucl. Data Tables* **1982**, *26*, 483.
(33) Krijn, J.; Baerends, E. J. *Fit-Functions in the HFS-Method*; Internal Report (in Dutch); Vrije Universiteit: Amsterdam, 1984.
(34) Versluis, L.; Ziegler, T. *J. Chem. Phys.* **1988**, *88*, 322−328.
(35) Slater, J. C. *Quantum Theory of Assessment of VDD and Other Methods for Charge Analysis. 209 Molecules and Solids*; McGraw-Hill: New York, 1974; Table 4.
(36) Becke, A. D. *J. Chem. Phys.* **1986**, *84*, 4524−4529.
(37) Becke, A. *Phys. Rev. A* **1988**, *38*, 3098−3100.
(38) Vosko, S. H.; Wilk, L.; Nusair, M. *Can. J. Phys.* **1980**, *58*, 1200−1211.
(39) Perdew, J. P. *Phys. Rev. B* **1986**, *33*, 8822−8824.
(40) Fan, L.; Ziegler, T. *J. Chem. Phys.* **1991**, *94*, 6057−6063.
(41) Lenthe, E. v.; Ehlers, A. E.; Baerends, E. J. *J. Chem. Phys.* **1999**, *110*, 8943−8953.
(42) Lenthe, E. v.; Baerends, E. J.; Snijders, J. G. *J. Chem. Phys.* **1993**, *99*, 4597−4610.
(43) Lenthe, E. v.; Baerends, E. J.; Snijders, J. G. *J. Chem. Phys.* **1994**, *101* (11), 9783−9792.
(44) Lenthe, E. v.; Snijders, J. G.; Baerends, E. J. *J. Chem. Phys.* **1996**, *105* (15), 6505−6516.
(45) Lenthe, E. v.; et al. *Int. J. Quantum Chem.* **1996**, *57*, 281−293.
(46) Ziegler, T.; Rauk, A. *Theor. Chim. Acta* **1977**, *46*, 1−10.
(47) Ziegler, T.; Rauk, A. *Inorg. Chem.* **1979**, *18*, 1755−1759.
(48) Mayer, I. *Chem. Phys. Lett.* **1983**, *97*, 270−274.
(49) Bridgeman, A. J.; Cavigliasso, G. *Inorg. Chem.* **2002**, *41* (13), 3500−3507.
(50) Novozhilova, I. V.; Volkov, A. V.; Coppens, P. *Inorg. Chem.* **2004**, *43* (7), 2299−2307.
(51) Love, I. *J. Phys. Chem. A* **2006**, *110* (35), 10507−10512.
(52) Kalinowski, J. A.; Lesyng, B.; Thompson, J. D.; Cramer, C. J.; Truhlar, D. G. *J. Phys. Chem. A* **2004**, *108* (13), 2545−2549.
(53) Reed, A. E.; Weinstock, R. B.; Weinhold, F. *J. Chem. Phys.* **1985**, *83*, 735−746.
(54) Reed, A. E.; Curtiss, L. A.; Weinhold, F. *Chem. Rev.* **1988**, *88*, 899−926 and references cited therein.
(55) Reed, A. E.; Schleyer, P. v. R. *J. Am. Chem. Soc.* **1990**, *112*, 1434−1445.
(56) Hirshfeld, F. L. *Theor. Chim. Acta* **1977**, *44*, 129−138.
(57) Guerra, C. F.; Handgraaf, J.-W.; Baerends, E. J.; Bickelhaupt, F. M. *J. Comput. Chem.* **2004**, *25*, 189−210.
(58) Mulliken, R. S. *J. Chem. Phys.* **1955**, *23*, 1833−1846.
(59) Arotsky, J.; Symons, M. C. R. *Inorg. Chem.* **1963**, *2* (4), 880−880.
(60) Pasternack, R. F.; Piper, T. S. *Inorg. Chem.* **1963**, *2* (2), 429−430.
(61) Burdett, J. K.; Price, G. D.; Price, S. L. *J. Am. Chem. Soc.* **1982**, *104* (1), 92−95.
(62) Wood, J. S.; Greene, P. T. *Inorg. Chem.* **1969**, *8* (3), 491−497.
(63) Jorgensen, W. L.; Tirado-Rives, J. *J. Am. Chem. Soc.* **1988**, *110*, 1657−1666.
(64) Damm, W.; Frontera, A.; Tirado-Rives, J.; Jorgensen, W. L. *J. Comp. Chem.* **1997**, *18*, 1955−1970.
(65) Jorgensen, W. L. In *Encyclopedia of Computational Chemistry*; Schleyer, P. v. R., Ed.; Wiley: New York, 1998; Vol. 3, pp 1986−1989.
(66) Casewit, C. J.; Colwell, K. S.; Rappé, A. K. *J. Am. Chem. Soc.* **1992**, *114*, 10035−10046.
(67) Casewit, C. J.; Colwell, K. S.; Rappé, A. K. *J. Am. Chem. Soc.* **1992**, *114*, 10046−10053.